ACS OMEGA

http://pubs.acs.org/journal/acsodf

Article

Corrosion Resistance of Amorphous-Nanocrystalline Composite Structure Materials

Qijun Xia, Pengwei Ren, and Huimin Meng*

Cite This: *ACS Omega* 2023, 8, 3348−3353

Read Online

ACCESS | Metrics & More | Article Recommendations

ABSTRACT: The purpose of this paper is to investigate the corrosion resistance of different nanoscale microstructures in the same material system and propose a novel method to obtain high-performance materials. During the last 2 decades, microstructure refinement and microalloying have become the main methods to prepare high-performance materials. The tensile strength of nanocrystalline solid solutions can reach 2.3 gigapascal, which is more than 1 fold the strength of traditional steel. However, there are few studies about the corrosion resistance of different nanoscale microstructures. In this paper, coatings with different microstructures (nanocrystalline, amorphous, and amorphous-nanocrystalline composite) have been successfully prepared by electrodeposition in the same material system (nickel−phosphorus alloy). Electrochemical test and high-pressure corrosion immersion test were carried out. The results show that the material loss of amorphous-nanocrystalline coating (P = 9.2 wt %) is about 1/4 that of crystalline coating at 8 MPa. In the range of 0.1 and 8 MPa, the average acceleration effect of hydrostatic pressure on the corrosion rate was calculated to be 1.611×10^{-6} g·cm^{-2}·d^{-1}·MPa^{-1}.

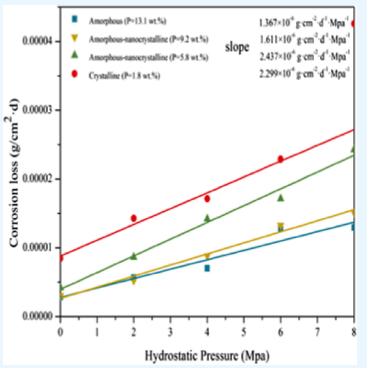

INTRODUCTION

In the past 2 decades, refinement of microstructure, nanocrystallization, and amorphism have become the main methods to obtain materials with high performance and special properties. Super steel was developed in the end of last century, the tensile strength and yield strength of which are achieved by means of fine crystallization, alloying, and pure purification. As a result, the strength and life of super steel were double that of traditional steel. Even some metals with nanocrystalline grains have ultrahigh strengths of more than 2 GPa.[1−4] For example, Li et al.[1] found that nanocrystalline nickel−cobalt solid solutions, although still a face-centered-cubic single phase, show tensile strengths of about 2.3 GPa with a respectable ductility of about 16 percent elongation to failure. However, after the success of super steel research and development, we are still faced with the problem of how to improve the strength, toughness, and life of structural materials. Especially with the continuous exploration of marine resources, the corrosion resistance of engineering equipment materials is facing high requirements. Moreover, due to the complex environment of deep-sea environment, the problem of corrosion life is difficult to test in the short term, and there are few studies on whether the corrosion life of super steel can be more than doubled. In order to prepare high-performance materials with both high wear resistance and high corrosion resistance, our team has proposed a novel method of nanocrystalline and amorphous composite microstructure, which can combine the advantages of high strength of nanocrystalline and high corrosion resistance of amorphous. In addition, it can avoid the poor corrosion resistance of nanocrystalline materials and the high brittleness of amorphous materials. However, it is difficult to produce materials with different microstructures in the same material system, and then accurate comparison of the relationship between the microstructure and properties is unrealistic. In order to overcome this problem, Ni−P alloy coating materials with nanocrystalline, amorphous, and amorphous-nanocrystalline composite microstructures were prepared by electrodeposition method in this work. According to previous studies, the phosphorus (P) content can regulate the microstructure of the Ni−P alloy from crystal to amorphous. Hou et al.[5] found that increasing the P content in the coating layer gradually shifts the coating structure from the microcrystalline transform to amorphous. The structure of electrodeposited Ni−P coatings is generally affected by plating parameters, including current density, electrolyte phosphate concentration, pH value, electrolyte composition, and temperature.[6,7] Correspondingly, the Ni−P coatings with different phosphorous contents and structure can be obtained by setting different parameters. The crystal structure of Ni−P coating can be divided into three categories

Received: November 2, 2022
Accepted: December 27, 2022
Published: January 10, 2023

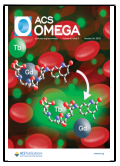

https://doi.org/10.1021/acsomega.2c07073
ACS Omega 2023, 8, 3348−3353

according to the phosphorus content. The first type when the phosphorus content is less than 5.2 wt %, the coating is crystal structure. In the second class, when the phosphorus content is between 5.2 and 10.2 wt %, the coating is amorphous and nanocrystalline composite structure. In the third class, when the phosphorus content is greater than 10.2 wt %, the coating is obviously amorphous structure. In previous research, our group found that the wear resistance of the amorphous-nanocrystalline Ni−P alloy was 7.4 times that of the amorphous Ni−P alloy and 3.1 times that of the nanocrystalline Ni−P alloy.[8] Therefore, the main research objective of this work is to compare the corrosion resistance of three different types of coatings. The coatings with nanocrystalline, amorphous-nanocrystalline composite, and amorphous microstructures were obtained by electrodeposition of Ni−P coatings on low carbon steel by controlling the pH value and current density. The coatings have been characterized by measuring the composition, observing the surface morphology, and analyzing the microstructure. Moreover, a series of electrochemical corrosion tests and high-pressure immersion corrosion tests were carried out. Due to the hydrostatic pressure factor in the marine environment, different hydrostatic pressures are set in the immersion experiment.

MATERIALS AND METHODS

Figure 1 shows the electroplating apparatus. The equipment includes a collector magnetic mixer, a DC power supply, and a

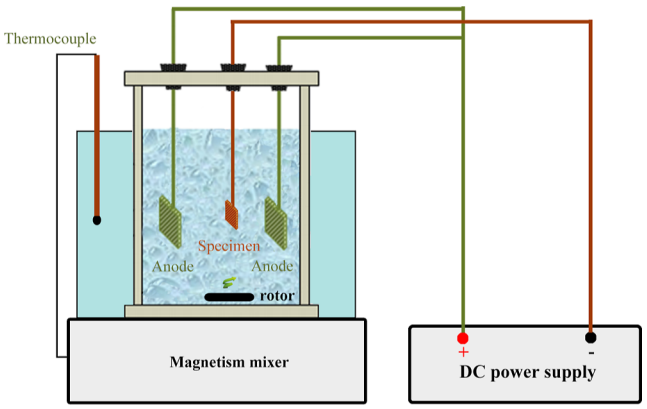

Figure 1. Schematic diagram of the instrument.

plating tank. The plating substrate is low carbon steel (Q235) with a plane size of 10 × 10 mm and thickness of 2 mm. The horizontal distance between the negative electrode and the two pure nickel (99.99%) anodes was 3 cm during plating. The magnetic rotor rotates at a constant speed at the bottom of the plating tank. The samples were abraded using sandpapers up to 1000 grit, then degreased by acetone, and further ultrasonically cleaned in deionized water. After pickling and activation, the specimens were immersed in the electroplating bath. The electroplating current density and pH were 20−60 mA/cm^2 and 0.8−1.6, respectively. In the process of electroplating, it is necessary to continuously add sulfuric acid solution to adjust the pH value of the bath to keep stable. The electroplating solution composition is nickel sulfate (240 g/L), nickel chloride (28 g/L), boric acid (30 g/L), phosphoric acid (6 g/L), and emulsifier (35 ppm) according to previous research.[8]

The surface of the deposited sample was characterized by field emission scanning electron microscopy (SUPRA55, USA). At the same time, the composition of the deposited sample was determined by energy-dispersive spectrometry (EDS). The microstructure morphology of coatings was studied by transmission electron microscopy (TEM) (Tecnai G2 F30) at 200 kV. The grain size of the sample was analyzed by XRD (Cu Kα radiation, Bruker D8 Discover). As for the high-pressure immersion test, 3.5 wt % NaCl solution was used as the immersion environment at 25 ± 2 °C. The weight loss rate of Ni−P coating was calculated after immersion for 7 days at different high pressures (0.1, 2, 4, 6, and 8 MPa). The autoclave was used to simulate the immersion corrosion under deep-sea environment. After the standardized treatment of the immersion experiment, the samples were weighed and marked with numbers. The samples were placed in an autoclave, sealed, and filled with nitrogen. The amount and pressure of nitrogen were controlled by the pressure gauge on the autoclave. After the immersion experiment, the samples were cleaned with deionized water. A brush was used to remove corrosion products from the surface of the sample. Finally, ultrasonic cleaning was carried out in deionized water. After the standardized treatment of the corrosion sample, the weight of the corroded sample was recorded. Electrochemical measurements were performed using a three-electrode cell to determine the electrochemical corrosion resistance in 3.5 wt % NaCl solution. The working electrodes were sealed with epoxy resin, leaving only an end surface (with a surface area of about 1 cm^2) exposed to corrosion medium. At the same time, platinum (99.9%) counter electrode served as the auxiliary electrode, and a saturated calomel reference electrode was also used in the system. The corrosion tests were carried out by a CHI660E machine in 3.5 wt % NaCl solution. Potentiodynamic polarization tests were employed to determine the corrosion properties of the obtained Ni−P films, and the scan rate was chosen to be 1 mV/s. Before the polarization tests, the open-circuit potential (OCP) of the films in 3.5 wt % NaCl solution was monitored after the films were adjusted to instrument parameters. The scan rate was chosen to be 0.01 V/s. Electrochemical impedance spectroscopy (EIS) was performed at OCP with a sinusoidal amplitude of 10 mV and a frequency range of 10^5 and 10^{-1} Hz. The free corrosion potential of the samples was continuously recorded for 1000 s before each EIS experiment. The impedance plots were interpreted by ZSimpWin software with a suitable fitting procedure.

RESULTS AND DISCUSSION

Figure 2 shows the previous research studies.[9] The crystal structure of Ni−P coating can be divided into three categories according to phosphorus content. In the first type, when the phosphorus content is less than 5.2 wt %, the coating is crystal structure. In the second class, when the phosphorus content is between 5.2 wt % and 10.2, the coating is amorphous and nanocrystalline composite structure. In the third class, when the phosphorus content is greater than 10.2 wt %, the coating is obviously amorphous structure. By adjusting the current density and pH value, the coatings with different P contents (sample 1, sample 2, sample 3, and sample 4) were obtained. The coatings were analyzed by EDS. The results show that the contents of phosphorus of samples 1, 2, 3, and 4 are 3.2, 5.8, 8, and 13.1 wt %, respectively. For sample 4 with a phosphorus content of 13.1 wt %, the diffusion peak near 2θ = 45° indicates that the crystal structure of the sample is amorphous. For sample 1, the narrower and sharper crystalline nickel (111)

https://doi.org/10.1021/acsomega.2c07073
ACS Omega 2023, 8, 3348−3353

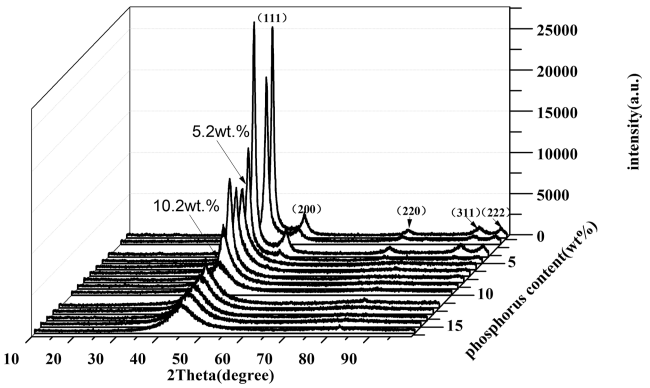

Figure 2. XRD pattern of Ni−P deposits with its different phosphorus contents.

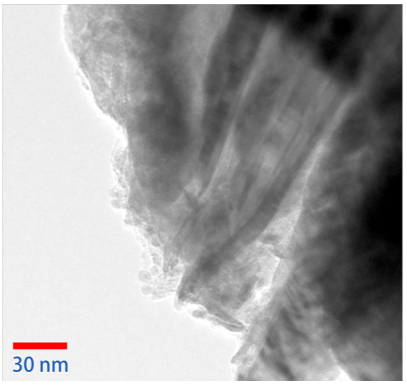

Figure 4. High-resolution TEM images of amorphous-nanocrystalline coatings.

features indicate that the sample has a crystalline structure. Samples 2 and 3 have both crystalline and amorphous characteristics. The full width at half-maximum of the diffraction peak decreases with the decrease of phosphorus content in the coating, which is related to the existence of nanocrystals.[10] According to the literature, the impurity of P will occupy octahedral interstitial sites, which will break the long-range order of Ni crystals.

As shown in Figure 3, Ni−P layers with different phosphorus contents, such as crystalline layer, amorphous nanocomposite film, and amorphous coating, have different microstructures. The coating exhibited homogeneous small nodular structures at low phosphorus content (crystalline) (Figure 3a). The Ni−P coatings with phosphorus contents of 5.8 and 8 wt % (amorphous-nanocrystalline composite) have a large nodular area containing a large number of small nodular cells (Figure 3b,c). At the surface of 13.1 wt % (amorphous) coating, all small nodular structures vanished and were replaced by plain amorphous grain structures (Figure 3d). Figure 4 illustrates the existing forms of nanocrystalline and amorphous structures in the amorphous-nanocrystalline coating. The nanocrystals are surrounded by amorphous structures, and in the corrosive environment, the amorphous structure of the coating can protect the nanocrystals.

Figure 5a illustrates the electrochemical polarization curves of the substrate and corresponding Ni−P coatings. Apparently, the corrosion potential of the electrodeposited Ni−P coating (crystalline, amorphous-nanocrystalline composite, and amorphous) is higher than that of the substrate (−0.625 V). The corrosion potential of Ni−P deposits is positively shifted from −0.460 to −0.471 V with increasing amorphous.[11] After standard Tafel extrapolation in the polarization curves, the corrosion current density (I_{corr}) of different coatings was acquired, as shown in Figure 5b. The figure shows that the current density gradually decreases with the increase of *P* content. The corrosion current density of amorphous coatings is lower than those of crystalline and amorphous-nanocrystalline coatings. However, when the phosphorus content is about 9 wt %, the corrosion current density of the amorphous-nanocrystalline coating is close to that of the amorphous coating.[12,13] The corrosion potentials (E_{corr}) and corrosion current densities (I_{corr}) of several representative samples are summarized in Table 1.

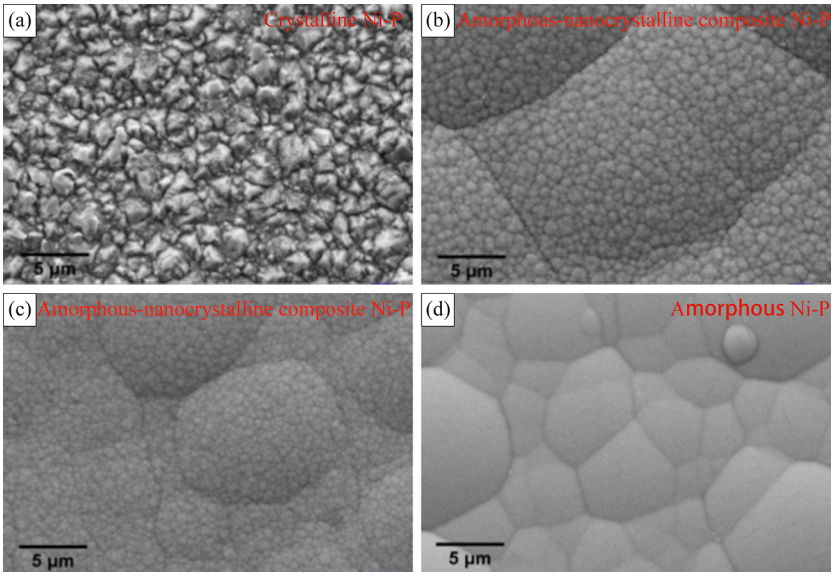

Figure 3. Surface morphology of Ni−P coatings with different phosphorus contents: (a) *P* = 3.2 wt %; (b) *P* = 5.8 wt %; (c) *P* = 8 wt %; (d) *P* = 13.1 wt %.

https://doi.org/10.1021/acsomega.2c07073
ACS Omega 2023, 8, 3348−3353

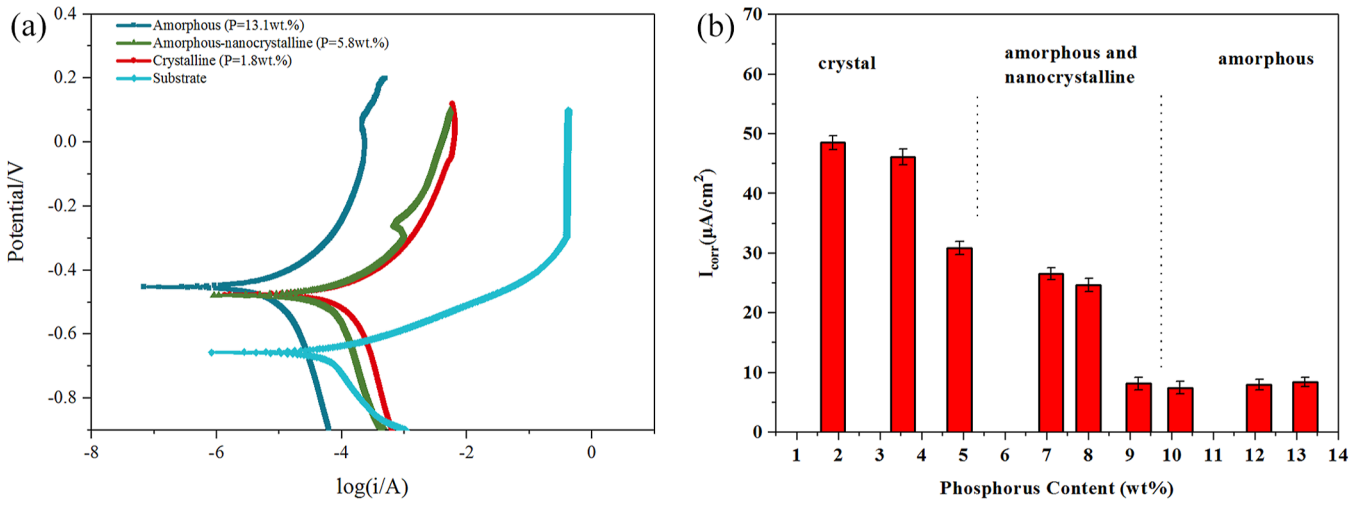

Figure 5. (a) Polarization curve and (b) self-corrosion current analysis for different kinds of coatings under 0.1 MPa.

Table 1. Corrosion Parameter Analysis Results of Nyquist Diagrams by Zsimpwin Software and the Analysis of Polarization Curves

material	morphology	R_{ct}(kΩ/cm^2)	I_{corr}(μ A/cm^2)	E_{corr} (V)
Ni−P(P = 13.1 wt %)	amorphous	24.9	8.4	−0.460
Ni−P(P = 9.2 wt %)	amorphous-nanocrystalline	4.7	9.1	−0.465
Ni−P(P = 5.6 wt %)	amorphous-nanocrystalline	3.6	27.2	−0.468
Ni−P(P = 1.8 wt %)	crystal	1.2	48.3	−0.471
substrate: carbon steel	crystal	1.0	69.7	−0.625

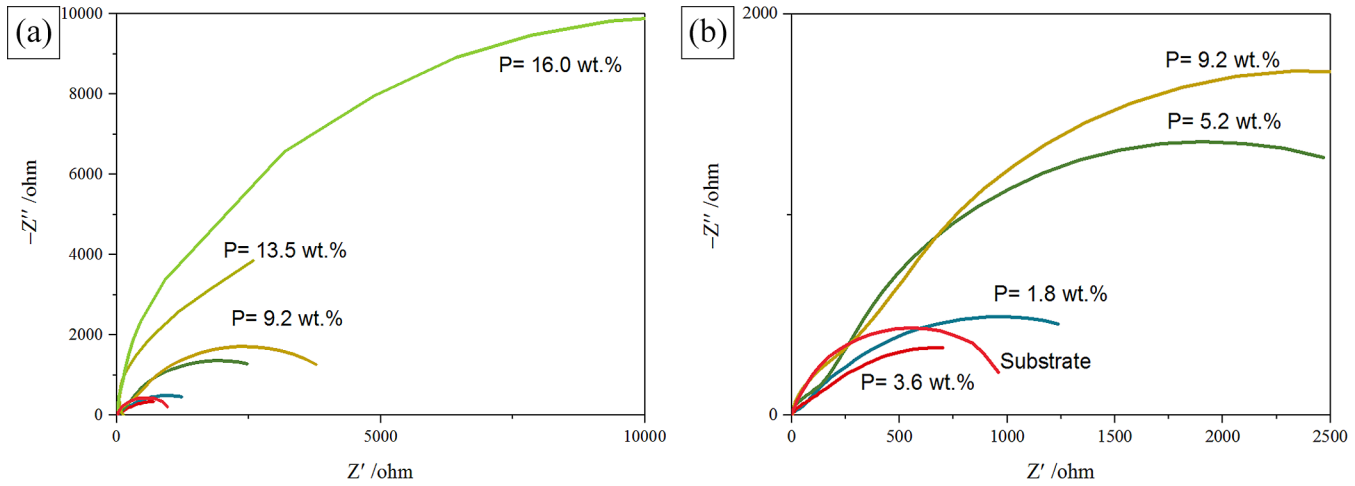

Figure 6. Nyquist diagrams of electrodeposited Ni−P coatings measured under immersion in 3.5 wt % NaCl solution: (a) Nyquist diagrams; (b) locally enlarged image.

As far as Ni−P coatings prepared in the present study are concerned, the corrosion current density and correspondingly the corrosion potentials are various due to the microstructure. Meanwhile, the emergence of the amorphous structure appears to significantly improve the corrosion resistance. The crystal Ni−P coating has a high value of corrosion current density. The corrosion behavior of Ni−P films thus primarily depends on the quantity and distribution of nanocrystalline in the amorphous matrix phase.

EIS spectra of Ni−P coatings conducted at OCP are shown in Figure 6. The plots of Nyquist spectra in Figure 6a,b give typical semicircles. The diameters of these semicircles vary with the phosphorus content. The high phosphorus content of amorphous Ni−P coatings shows a larger charge-transfer resistance than the crystal coating and amorphous-nanocrystalline composite coatings (Table 1). By comparing the electrochemical parameters from the EIS data of Ni−P coatings in 3.5 wt % NaCl solution and XRD patterns, it can be seen that the nanocrystalline coating has more grain boundaries, and hence it is less protective. The coatings become denser and less porous by increasing the amorphous region.[14]

The results of the high-pressure immersion test of different coatings are shown in Figure 7. Yang et al.[15,16] studied the effect of hydrostatic pressure on the pitting performance of X70 pipeline steel, and the results showed that the hydrostatic pressure promoted the initiation and development of pitting corrosion, and in addition, the hydrostatic pressure promoted

https://doi.org/10.1021/acsomega.2c07073
ACS Omega 2023, 8, 3348−3353

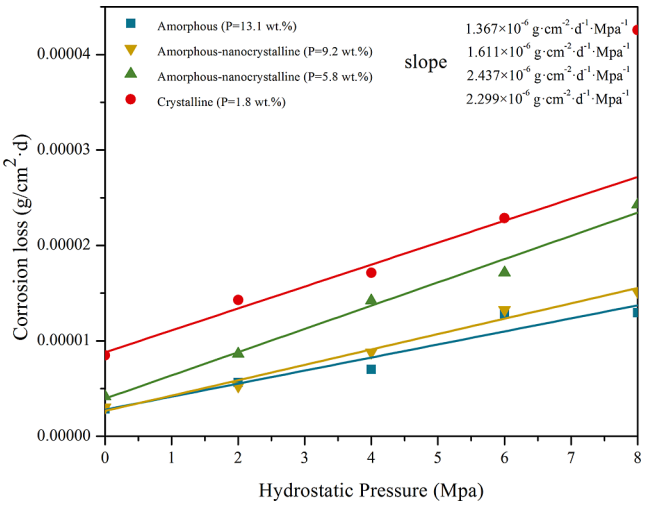

Figure 7. Corrosion rate and average acceleration effect of the hydrostatic pressure of coating.

the penetration and adsorption of chloride ions in the embroider layer, which made the corrosion rate increase with the increase of hydrostatic pressure. The results of high-pressure immersion test show that the corrosion loss of the coatings increases with the increase in hydrostatic pressure. The corrosion rate of the amorphous-nanocrystalline coating (P = 9.2 wt %) is linearly related to the hydrostatic pressure (i.e., sea water depth), as shown in the equation

$$W = 2.651 \times 10^{-6} + 1.611 \times 10^{-6} P$$

where W is the corrosion rate ($g \cdot cm^{-2} \cdot d^{-1}$) and P is the hydrostatic pressure (MPa). It is worth noting that the average acceleration of the corrosion rate of coatings within the range of 0.1 and 8 MPa hydrostatic pressure is 1.611×10^{-6} $g \cdot cm^{-2} \cdot d^{-1} \cdot MPa^{-1}$, that is, the corrosion rate at the seawater depth ranging from the sea level to 800 m increases 1.611×10^{-6} $g \cdot cm^{-2} \cdot d^{-1}$ for every 1 MPa hydrostatic pressure (i.e., 100 m seawater depth).

This indicates that the hydrostatic pressure of seawater has a significant negative effect on the corrosion resistance of the coating. The negative effect of high hydrostatic pressure is significantly reduced compared with that of the crystalline coating and amorphous-nanocrystalline coatings (P = 5.8 wt %). Nanocrystalline coating has more grain boundaries, so it has poor protection. With the increase of the amorphous region, the density of the coating increases, the porosity decreases, and the negative effect of high hydrostatic pressure decreases. At each hydrostatic pressure, the crystalline coating has the maximum corrosion loss, which is about twice that of the amorphous coating. For the amorphous-nanocrystalline coating, the corrosion loss decreases with the increase of phosphorus content. The corrosion loss of the coating with high phosphorus content (P = 9.2 wt %) is close to that of the amorphous coating under hydrostatic pressure and even lower than that of the amorphous coating at 600 m sea depth. Amorphous-nanocrystalline coatings (P = 9.2 wt %) and amorphous coatings show good corrosion resistance. In previous studies, our team had found that amorphous-nanocrystalline coatings have better wear resistance. The wear resistance of the amorphous-nanocrystalline Ni−P alloy was 7.4 times of that of the amorphous Ni−P alloy and 3.1 times of that of the nanocrystalline Ni−P alloy. Therefore, the combination of amorphous and nanocrystalline materials with good wear and corrosion resistance can become good service materials in abrasive seawater environment.

CONCLUSIONS

1 By adjusting the process parameters of electrodeposition (current density, etc.) to control the P content, three different structures (crystalline, amorphous-nanocrystalline, and amorphous) of Ni−P coatings were obtained successfully. The corrosion properties of three different structures were compared.

2 The corrosion rate increases with increasing hydrostatic pressure (i.e., seawater depth). For the amorphous-nanocrystalline coatings (P = 9.2 wt %), the average acceleration effect of hydrostatic pressure on corrosion rate in the range of 0.1 and 8 MPa is 1.611×10^{-6} $g \cdot cm^{-2} \cdot d^{-1} \cdot MPa^{-1}$.

3 With the increase of phosphorus content of the amorphous-nanocrystalline coating, the amorphous region increases, the density of the coating increases, the porosity decreases, and the negative effect of high hydrostatic pressure decreases. The corrosion weight loss and the seawater pressure acceleration rate of the amorphous-nanocrystalline coating (P = 9.2 wt %) are similar to those of the amorphous coating at various depths of seawater. In combination with the previous studies on the wear resistance of three kinds of coatings, it can be concluded that the amorphous-nanocrystalline composite may be a direction for the development of high strength and long-life high performance structural materials. In the next step of work, the tribocorrosion properties of the three coatings under different hydrostatic pressure and potential will be tested, and the evolution of the wear mechanism under different seawater depths will be obtained.

AUTHOR INFORMATION

Corresponding Author

Huimin Meng − *Corrosion and Protection Center, Institute of Advanced Materials and Technology, University of Science and Technology Beijing, Beijing 100083, China*; Phone: +86-010-6233-2548; Email: menghm16@126.com

Authors

Qijun Xia − *Corrosion and Protection Center, Institute of Advanced Materials and Technology, University of Science and Technology Beijing, Beijing 100083, China*; orcid.org/0000-0002-0643-2889

Pengwei Ren − *Corrosion and Protection Center, Institute of Advanced Materials and Technology, University of Science and Technology Beijing, Beijing 100083, China*

Complete contact information is available at: https://pubs.acs.org/10.1021/acsomega.2c07073

Notes

The authors declare no competing financial interest.

ACKNOWLEDGMENTS

This research was funded by the Major State Basic Research Development Program of China (973 Program), grant number 2014CB643302.

https://doi.org/10.1021/acsomega.2c07073
ACS Omega 2023, 8, 3348−3353

REFERENCES

(1) Li, H.; Zong, H.; Li, S.; Jin, S.; Chen, Y.; Cabral, M. J.; Chen, B.; Huang, Q.; Chen, Y.; Ren, Y.; Yu, K.; Han, S.; Ding, X.; Sha, G.; Lian, J.; Liao, X.; Ma, E.; Sun, J. Uniting tensile ductility with ultrahigh strength via composition undulation. *Nature* **2022**, *604*, 273−279.
(2) He, B. B.; Hu, B.; Yen, H. W.; Cheng, G. J.; Wang, Z. K.; Luo, H. W.; Huang, M. X. High dislocation density-induced large ductility in deformed and partitioned steels. *Science* **2017**, *357*, 1029−1032.
(3) Du, X. H.; Li, W. P.; Chang, H. T.; Yang, T.; Duan, G. S.; Wu, B. L.; Huang, J. C.; Chen, F. R.; Liu, C. T.; Chuang, W. S.; Lu, Y.; Sui, M. L.; Huang, E. W. Dual heterogeneous structures lead to ultrahigh strength and uniform ductility in a Co-Cr-Ni medium-entropy alloy. *Nat. Commun.* **2020**, *11*, 2390.
(4) Jiang, S.; Wang, H.; Wu, Y.; Liu, X.; Chen, H.; Yao, M.; Gault, B.; Ponge, D.; Raabe, D.; Hirata, A.; Chen, M.; Wang, Y.; Lu, Z. Ultrastrong steel via minimal lattice misfit and high-density nanoprecipitation. *Nature* **2017**, *544*, 460−464.
(5) Hou, K.-H.; Jeng, M.-C.; Ger, M.-D. A study on the wear resistance characteristics of pulse electroforming Ni-P alloy coatings as plated. *Wear* **2007**, *262*, 833−844.
(6) Yuan, X.; Sun, D.; Yu, H.; Meng, H.; Fan, Z.; Wang, X. Preparation of amorphous-nanocrystalline composite structured Ni-P electrodeposits. *Surf. Coat. Technol.* **2007**, *202*, 294−300.
(7) Pillai, A. M.; Rajendra, A.; Sharma, A. K. Electrodeposited nickel-phosphorous (Ni-P) alloy coating: an in-depth study of its preparation, properties, and structural transitions. *J. Coat. Technol. Res.* **2012**, *9*, 785−797.
(8) Xia, Q.; Ren, P.; Meng, H. High performance of amorphous nanocrystalline composite structure materials. *J. Mater. Res. Technol.* **2022**, *18*, 4479−4485.
(9) Zhang, S.; Cao, F.; Chang, L.; Zheng, J.; Zhao, Z.; Zhang, J.; Cao, C. Electrodeposition of high corrosion resistance Cu/Ni-P coating on AZ91D magnesium alloy. *Appl. Surf. Sci.* **2011**, *257*, 9213−9220.
(10) Juraić, K.; Gracin, D.; Djerdj, I.; Lausi, A.; Ceh, M.; Balzar, D. Structural analysis of amorphous-nanocrystalline silicon thin films by grazing incidence X-ray diffraction. *Nucl. Instrum. Methods Phys. Res., Sect. B* **2012**, *284*, 78−82.
(11) Li, S.; Zuo, Y.; Ju, P. Erosion-corrosion resistance of electroplated Co-Pd film on 316L stainless steel in a hot sulfuric acid slurry environment. *Appl. Surf. Sci.* **2015**, *331*, 200−209.
(12) Shu, X.; Wang, Y.; Liu, C.; Aljaafari, A.; Gao, W. Double-layered Ni-P/Ni-P-ZrO 2 electroless coatings on AZ31 magnesium alloy with improved corrosion resistance. *Surf. Coat. Technol.* **2015**, *261*, 161−166.
(13) Liu, W.-H.; Shieu, F.-S.; Hsiao, W.-T. Enhancement of wear and corrosion resistance of iron-based hard coatings deposited by high-velocity oxygen fuel (HVOF) thermal spraying. *Surf. Coat. Technol.* **2014**, *249*, 24−41.
(14) Rabizadeh, T.; Allahkaram, S. R.; Zarebidaki, A. An investigation on effects of heat treatment on corrosion properties of Ni-P electroless nano-coatings. *Mater. Des.* **2010**, *31*, 3174−3179.
(15) Yang, Z.; Kan, B.; Li, J.; Qiao, L.; Volinsky, A. A.; Su, Y. A statistical study on the effect of hydrostatic pressure on metastable pitting corrosion of X70 pipeline steel. *Materials* **2017**, *10*, 1307.
(16) Yang, Z. X.; Kan, B.; Li, J. X.; Su, Y. J.; Qiao, L. J. Hydrostatic pressure effects on corrosion behavior of X70 pipeline steel in a simulated deep-sea environment. *J. Electroanal. Chem.* **2018**, *822*, 123−133.

https://doi.org/10.1021/acsomega.2c07073
ACS Omega 2023, 8, 3348−3353